Supporting information for
Self-assembled nanoparticle dimer antennas for plasmonic-enhanced single-molecule fluorescence detection at micromolar concentrations

Deep Punj, Raju Regmi, Alexis Devilez, Robin Plauchu, Satish Babu Moparthi, Brian Stout, Nicolas Bonod, Hervé Rigneault, and Jérôme Wenger
CNRS, Aix-Marseille Université, Centrale Marseille, Institut Fresnel, UMR 7249, 13013 Marseille, France
Email: jerome.wenger@fresnel.fr

This document contains the following supporting information:

1 Wide field image of the sample

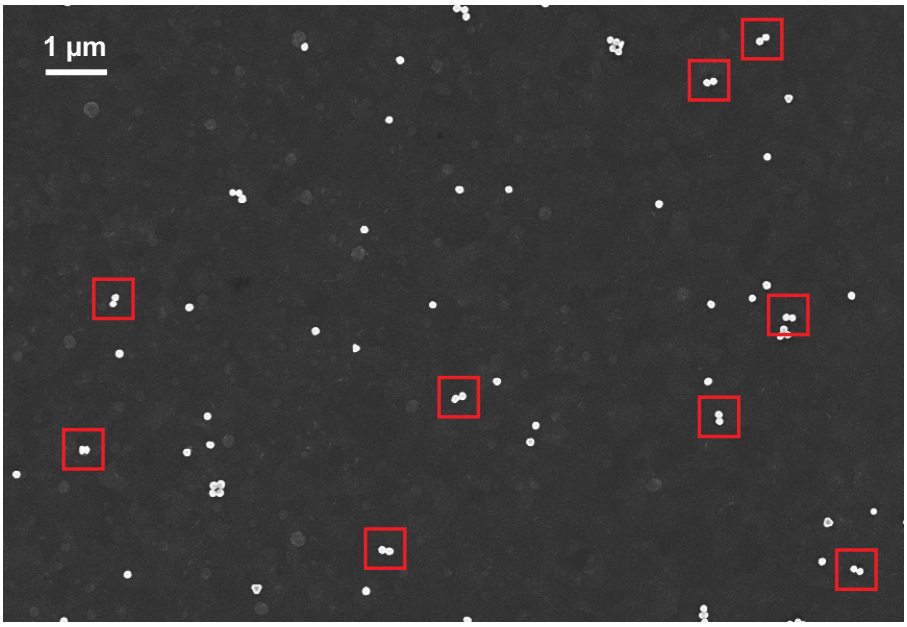

Figure S1: Scanning electron microscope image of the self-assembled dimer nanoparticle antennas on ITO substrate. Several dimer antennas are readily identified on this zone, as highlighted by red boxes. These relevant antennas are then further analyzed on the fluorescence correlation spectroscopy experiment.

2 Effective refractive index for the surrounding medium

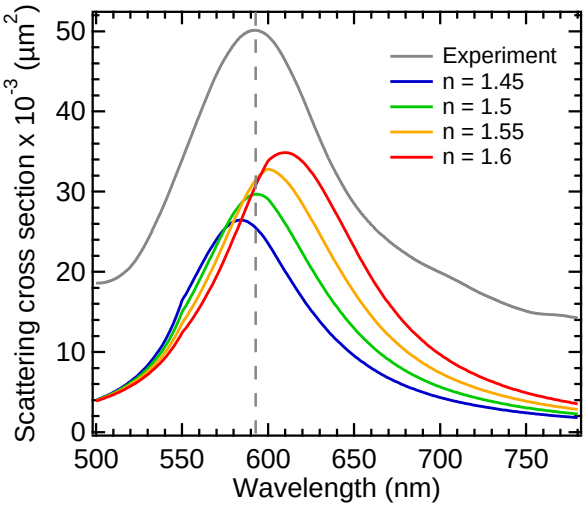

Figure S2: Determination of the surrounding medium effective refractive index n_{eff} used in Mie theory computations so as to match the local surface plasmon resonance wavelength of a single 80 nm spherical nanoparticle. The experimental scattering spectra (averaged over an ensemble of nanoparticles) is plotted in gray and vertically shifted. The case $n_{eff} = 1.5$ provides the best matching to the experimental data. Additionally, this finding is confirmed by the average between the refractive index of the water superstrate ($n = 1.33$) and the ITO substrate ($n = 1.81$) at 600 nm.

3 Gap size estimates

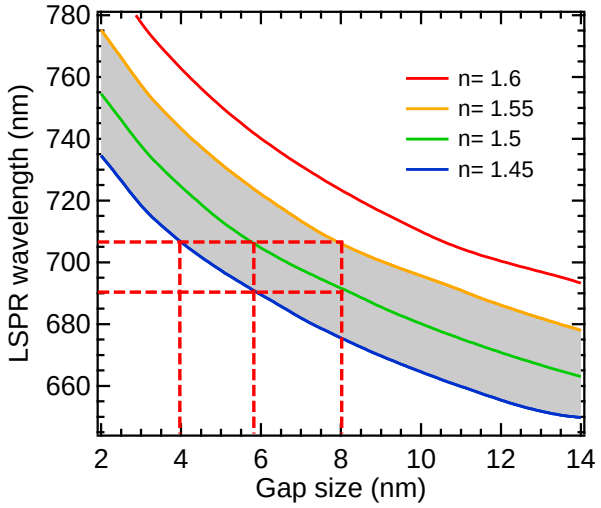

Figure S3: Determination of the gap size from the longitudinal plasmon resonance (LSPR) wavelength. The graph displays the LSPR wavelength for a dimer of 80 nm nanoparticles as function of the gap size, computed according to Mie theory [1]. Different effective refractive indexes for the surrounding medium are also considered; the case $n_{eff} = 1.5$ provides the best matching to the experimental observations for the scattering spectrum of a single nanoparticle (Fig. S2) and the dimer (Fig. 1e,f). The dashed horizontal lines indicate the spectral interval of the experimentally observed LSPR values, which correspond to a gap size estimate of 6 ± 2 nm.

4 PEG spacer reduces the red-shift of the dimer LSPR resonance

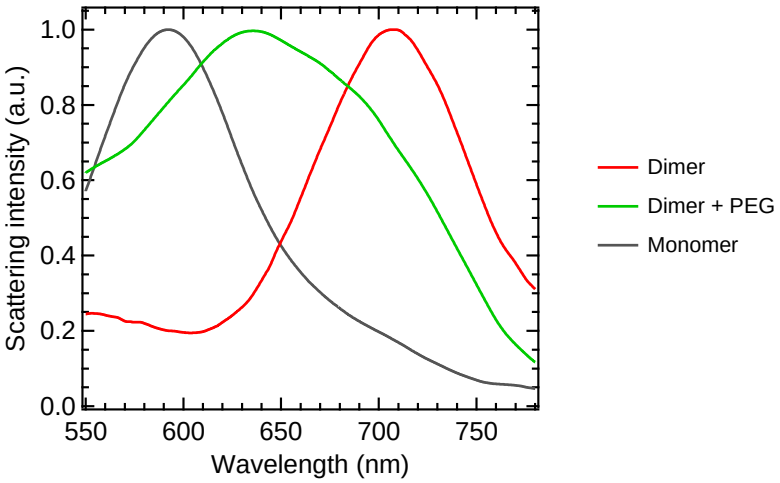

Figure S4: Normalized dark-field scattering spectra in the presence of a supplementary PEG spacer surrounding the 80 nm nanoparticles (green line). A significant blue-shift is observed as compared to the dimer antenna without PEG (red line). This blue-shift indicates a larger gap size of $\sim$ 13 nm according to the calibration graph in Fig. S3 and the PEG refractive index of 1.46.

5 Absorption, scattering and extinction cross-sections

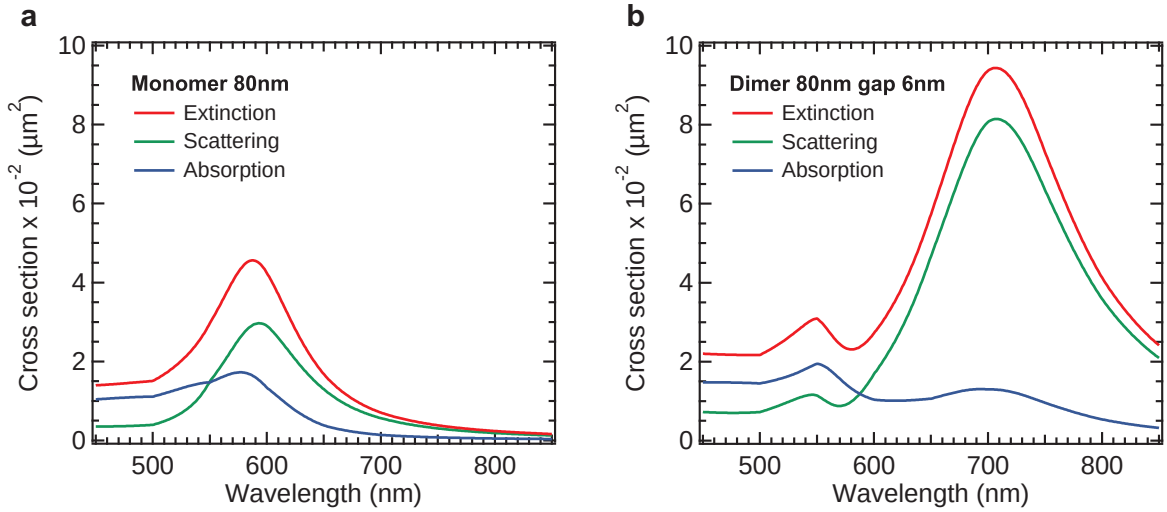

Figure S5: Absorption (blue), scattering (green) and extinction (red) cross-sections computed following Mie theory for a single 80 nm gold nanoparticle (a) and a dimer of 80 nm nanoparticles separated by a 6 nm gap (b) assuming an effective homogeneous refractive index of $n_{eff} = 1.5$. For both systems, scattering dominates over absorption in the spectral range 630-700nm considered in the experiments.

6 FCS analysis

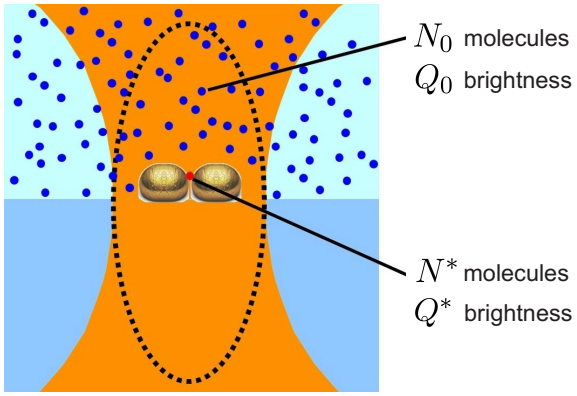

Figure S6: Notations used in the FCS analysis.

The experiments on nanoparticle antennas covered by a solution of fluorescent molecules correspond to the case of having two species with different numbers of molecules and fluorescence brightness as illustrated on Fig. S6: N^* molecules are present in the dimer hot spot volume and experience a brightness Q^*, while N_0 (background) molecules with brightness Q_0 are diffusing away from the hot spot but still in the diffraction-limited confocal volume. The fluorescence intensity correlation function can be written (see pages 75-81 of [2]):

$$G(\tau) = \frac{\langle F(t).F(t+\tau)\rangle}{\langle F(t)\rangle^2} = 1 + \frac{N^*Q^{*2}G_{d*}(\tau) + N_0Q_0^2G_{d0}(\tau)}{(N^*Q^* + N_0Q_0)^2} \tag{1}$$

where $G_{d*}(\tau)$ and $G_{d0}(\tau)$ are the normalized functional forms of the correlation function for each species taken individually based on a three dimensional Brownian diffusion model:

$$G_{di}(\tau) = \frac{1 + n_{T,i}\exp\left(-\frac{\tau}{\tau_{b_T,i}}\right)}{(1+\tau/\tau_{d,i})\sqrt{1+s_i^2\,\tau/\tau_{d,i}}} \tag{2}$$

$n_{T,i}$ stands for the amplitude of the dark state population, $\tau_{b_T,i}$ the dark state blinking time, $\tau_{d,i}$ the mean residence time (set by translational diffusion) and s_i the ratio of transversal to axial dimensions of the analysis volume. The shape parameter is fixed to $s = 0.2$ to allow for direct comparison between diffusion times. This parameter was found to have a negligible influence on the estimates for N^* and Q^* which are the main goals of the paper.

Equation (1) indicates that the different fluorescent species contribute to the amplitude of $G(\tau)$ in proportion to the square of their relative fluorescence brightness. This is an important element as it enables extracting a significant FCS signal from a low number of molecules N^* under conditions of large background N_0, Q_0. A purely linear technique -such as time correlated single photon counting

TCSPC- experience more difficulties in extracting the useful information from the hotspot (see Section 10 and 11 for details).

Here we are primarily interested in quantifying the hotspot fluorescence brightness Q^* and the hotspot detection volume for FCS, which (for a known sample concentration) amounts to the number of molecules in the hotspot N^*. This quantification does not require the complete temporal information from the FCS correlation, the value of the correlation function at zero lag time will be sufficient:

$$G(0) = 1 + \frac{N_0 Q_0^2 + N^* Q^{*2}(1 + n_T^*)}{(N_0 Q_0 + N^* Q^*)^2} \tag{3}$$

Here we already made the simplification that the amplitude n_T of the dark state population is negligible for molecules away from the hot spot, as confirmed by confocal measurements and as expected for a dye with very short lifetime (with 200mM of methyl viologen the fluorescence lifetime of Alexa Fluor 647 is reduced to 300 ps) and under low excitation power (10 μW in continuous). For completeness, we keep considering a free parameter n_T^* for the dark state blinking amplitude in the case of the hotspot. As we will show below, this parameter reduces the fluorescence enhancement and volume reduction factors by $(1 + n_T^*)$, so the experimental values indicated in the document should be considered as conservative estimates.

In addition to the expression of $G(0)$, we use the known value of the average total fluorescence intensity F:

$$F = N_0 Q_0 + N^* Q^* \tag{4}$$

Inserting the result that $N^* Q^* = F - N_0 Q_0$ into Eq. (3), we obtain the expression

$$G(0) = 1 + \frac{N_0 Q_0^2 + (F - N_0 Q_0) Q^* (1 + n_T^*)}{F^2} \tag{5}$$

which only linearly depends on Q^*. Inverting this equation provides the fluorescence brightness and number of molecules in the hotspot:

$$Q^* = \frac{F^2 (G(0) - 1) - N_0 Q_0^2}{(F - N_0 Q_0)\,(1 + n_T^*)} \tag{6}$$

and

$$N^* = \frac{F - N_0 Q_0}{Q^*} = \frac{(F - N_0 Q_0)^2}{F^2 (G(0) - 1) - N_0 Q_0^2}\ (1 + n_T^*) \tag{7}$$

These expressions show that in addition to the experimentally measured parameters $F, G(0), n_T^*$, we also need to estimate the values of N_0, Q_0 to quantify N^*, Q^*. The fluorescence brightness away from the hot spot Q_0 is set according to the value found for the confocal reference Q_{conf}. More elaborate strategies can be used (as found in [3]) and lead to comparable results. To estimate the number of molecules N_0 in the background, we take advantage of the polarization response of dimer antennas, and consider the case of excitation polarization perpendicular to the dimer axis. In the case of perpendicular excitation we assume that two single 80 nm gold nanoparticles are excited collectively. According to the formulation of FCS under several laser spots [4], we can write $N_\perp^* = 2 \times N_{np}^*$ and

$Q^*_\perp = Q^*_{np}$ where N^*_{np} and Q_{np^*} are the number of molecules and brightness in the case of a single nanoparticle, which were calibrated independently in our previous work [5, 6] and confirmed by the experiments in Fig. 2. For individual 80 nm gold nanoparticles, we found a fluorescence enhancement $\eta_{F,np} = 60\times$ and a volume reduction $R_{V,np} = 1800\times$. Hence in the case of a dimer antenna for perpendicular polarization:

$$N^*_\perp = 2 \times \frac{N_{conf}}{R_{V,np}} \quad (8)$$

$$Q^*_\perp = \eta_{F,np} \times Q_{conf} \quad (9)$$

where N_{conf} and Q_{conf} are the number of molecules and brightness in the case of confocal reference. From here we can find out the background molecules N_0 using the relation $F_\perp = N_0 Q_0 + N^*_\perp Q^*_\perp$ which provides the information needed to complete the quantification in Eq.(6,7).

Lastly for trimers, we use the same procedure as in [5]: the number of emitters and brightness N_0, Q_0 for the molecules diffusing away from the hot spot are fixed according to the values found at the glass-water interface without nanoparticle, corrected by a factor of $C = 1 - 3(d/2w)^2$ to account for the screening induced by the nanoparticles (d is the nanoparticle diameter, w=280 nm is the laser beam waist at focus). Typically, C amounts to 0.94 for 80 nm nanoparticles.

	Confocal	**Dimer**		**Trimer**			
Excitation	Linear	Parallel	Perpendicular	0°	90°	+45°	-45°
F (kHz)	767	437	428	410	399	400	406
$G(0) - 1$	2.5e-4	0.048	0.007	0.035	0.023	0.031	0.021
N	4000	0.55	4.4	1.2	1.3	1.1	1.6
τ_d (μs)	64	1.9	3.6	1.9	1.7	1.6	1.7
n_T	-	0.4	-	0.2	0.15	0.3	0.1
τ_{b_T} (μs)	-	0.4	-	0.2	0.5	0.2	0.5
Q (kHz)	0.19	109	11.4	64	49	58	44
Fluorescence Enhancement		575	60	335	260	305	230
Volume Reduction		7300	900	3440	3050	3550	2450

Table S1: Fitting parameter results for the FCS curves obtained on dimer (Fig 2c) and trimer nanoantenna (Fig S8d). The experimental conditions are identical between cases: Alexa Fluor 647 concentration 13.3 μM with 200 mM of methyl viologen used as a chemical quencher, excitation power 10 μW with linear polarization. In the dimer case, there is no additional PEG layer, while for the trimer the PEG layer is present so as to maximize the enhancement factor (Fig 4a,c).

7 Correlation traces versus excitation polarization on a nanoparticle dimer

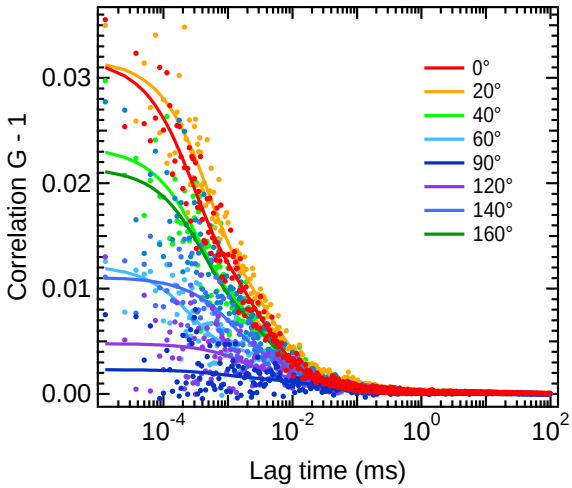

Figure S7: Fluorescence correlation functions (raw data) corresponding to the results plotted on Fig. 2d-f of the main document obtained for various angles θ of the laser polarization.

8 Experimental data on trimers of nanoparticles

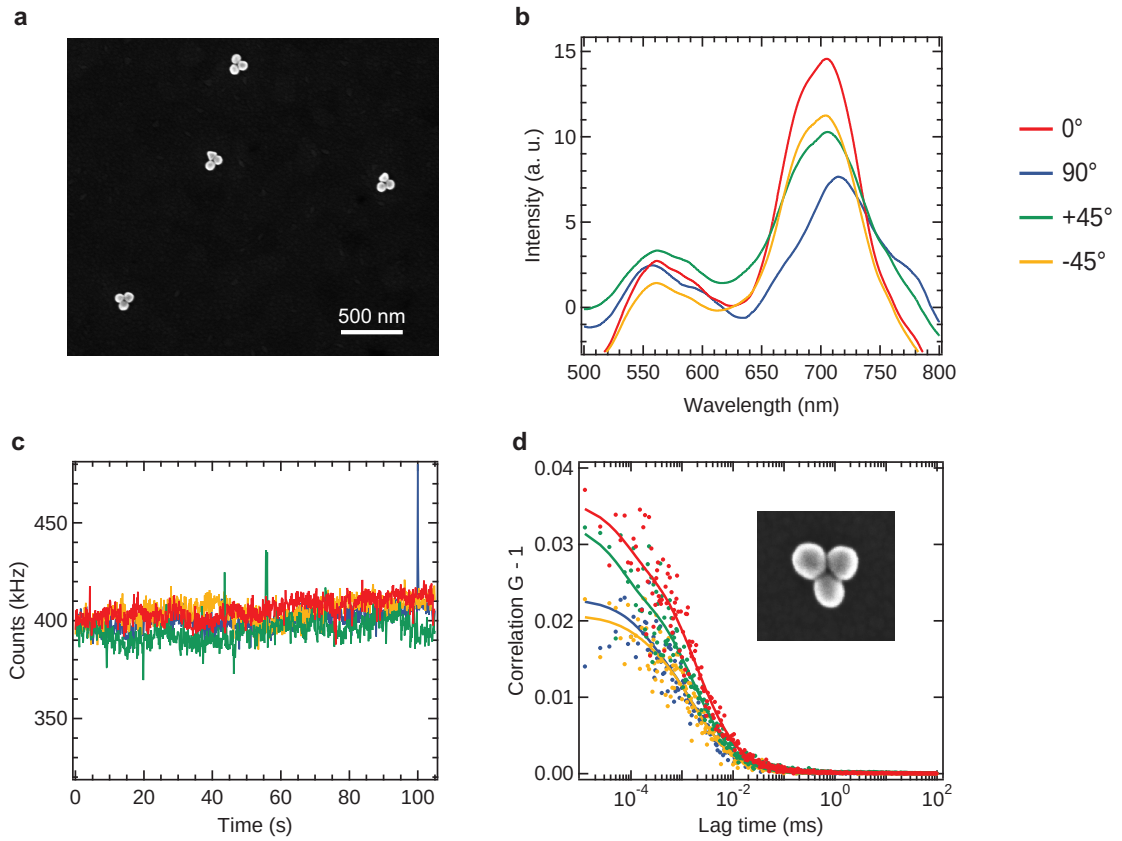

Figure S8: (a) Scanning electron image of self-assembled nanoparticle trimers. (b) Dark-field scattering spectra, normalized by the reference spectrum of the lamp, for different illumination polarizations. Due to the triangular shape of the trimer, only minor variations are seen with the polarization direction. No PEG was used in the experiment leading to these data. (c) Fluorescence intensity time trace and (d) FCS correlation function taken on a representative trimer antenna for different polarization orientations (same color code as in (b)). Again, minor variations with the polarization orientation are seen. The experimental conditions are identical to the ones in Fig. 2, with a concentration of Alexa Fluor 647 of 15 μM and 200 mM of methyl viologen, so that the correlation traces can directly be compared between the cases (confocal, dimer and trimer). Remarkably, the correlation amplitude for the trimer is higher than the confocal, indicating sub-wavelength confinement of light, and smaller that the dimer antenna, indicating a larger volume for the trimer as compared to the dimer.

9 Excitation intensity distribution on a trimer of nanoparticles

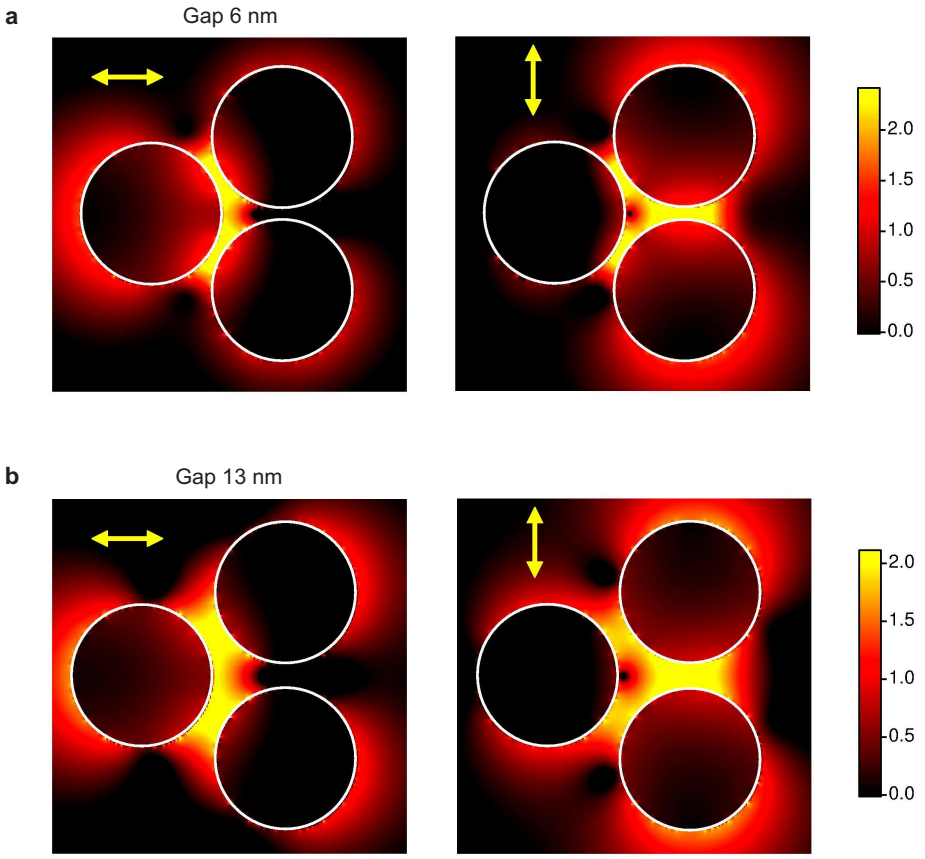

Figure S9: Finite-difference time-domain computation of the excitation intensity enhancement (log scale) for the trimer antenna in the equatorial planes of the nanoparticles for two different polarizations as indicated on the graphics. The wavelength is 633 nm, the particle size 80 nm and the gap is 6 nm for (a) and 13 nm for (b).

10 Fluorescence lifetimes and decay traces on dimer and trimer antennas

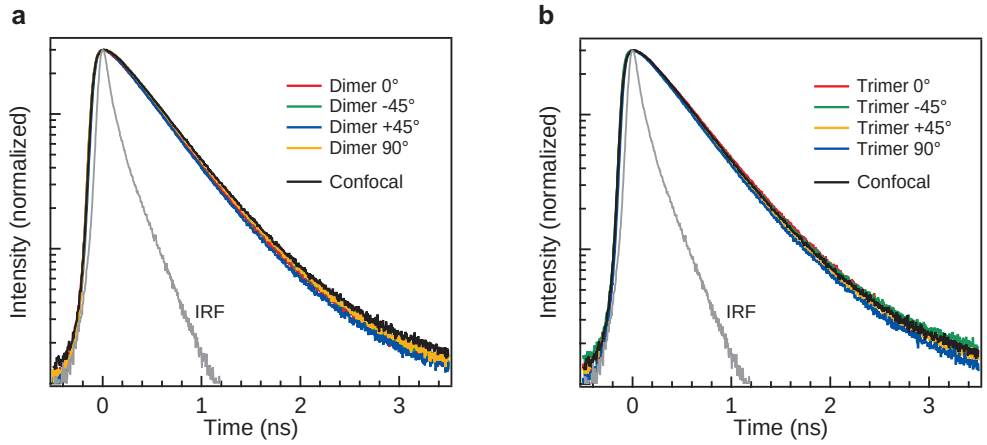

Figure S10: Normalized fluorescence decay traces under pulsed excitation for a dimer (a) and a trimer (b) antenna with different excitation polarizations. The black curve indicates the reference decay trace in confocal configuration when no antenna is present. It corresponds to a fluorescence lifetime of 300 ps in the presence of 200 mM of methylviologen (the IRF full width at half maximum is 120 ps). There might be a lifetime reduction due to the nanoantenna. However, due to the large fluorescence contribution from the N_0 molecules surrounding the antenna and the short lifetime of the dye, the effect is blurred and the determination of the lifetime reduction in the hot spot is impossible in this case. These findings stand in good agreement with the simulations shown in Fig. S11.

11 Simulations of FCS and TCSPC results

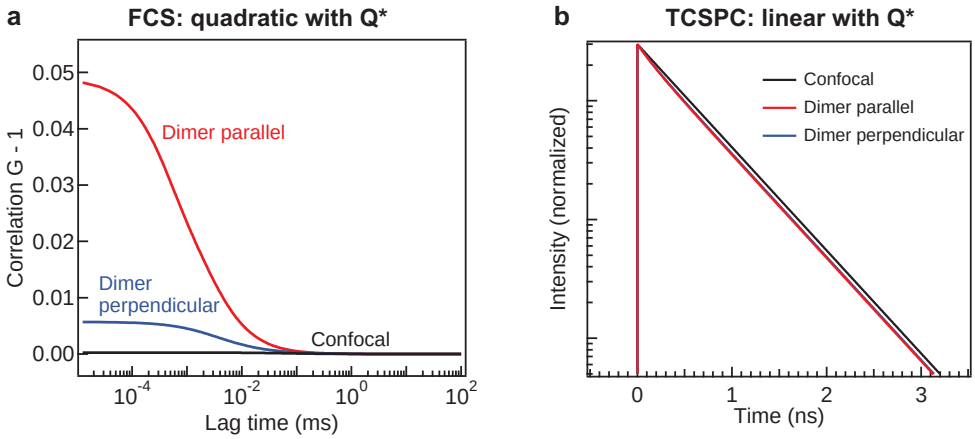

Figure S11: Simulated FCS and TCSPC data using only the parameters in Tab. S1. The simulated FCS data (a) should be compared to the experimental results Fig. 2c, and the TCSPC simulations (b) correspond to the case of Fig. S10a. The excellent agreement between simulations and experimental data provides an *a posteriori* validation of our results (enhancement factor and volume reduction). It also emphasizes the difficulty to extract the useful information from the antenna hotspot hidden in the TCSPC decay curve: while in FCS the hotspot contribution is quadratic with the brightness Q^* (Eq. 1), in TCSPC the dependence is linear.

12 Luminescence background when no fluorescent dye is present

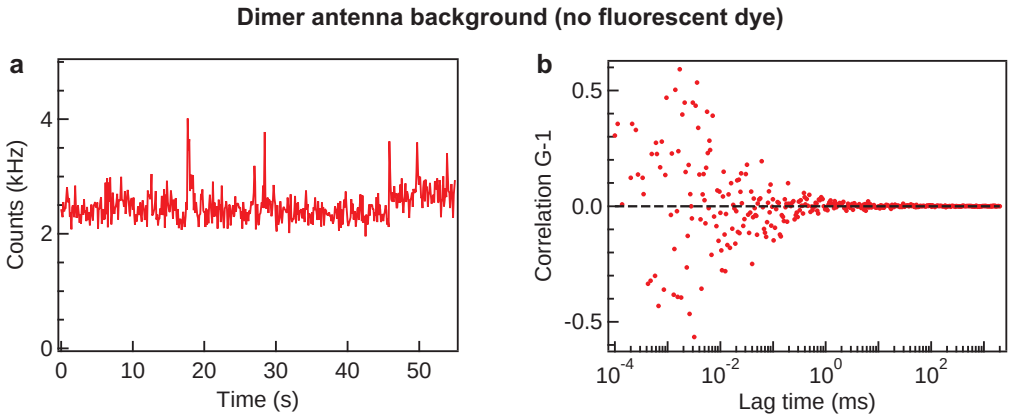

Figure S12: (a) Intensity trace and (b) correlation function on a dimer antenna covered with 200 mM methyl viologen in water solution. No fluorescent molecule is used in this experiment to record the level of luminescence background. White light extinction and laser scattering ensure the presence of a dimer antenna. The laser polarization is oriented along the dimer axis so as to maximize the detected luminescence level. A weak signal is detected on the avalanche photodiodes (a), and originates mainly from residual backscattered laser light after the filters and autoluminescence from the sample. Despite some peaks can be seen sometimes on the time trace, no correlation is found (b), as the FCS data is remarkably symmetric around the zero level. The total integration time for this trace is 200 s, with the same conditions as Fig. 2, S7 and S8.

References

[1] Stout, B.; Auger, J. C.; Devilez, A. Recursive T-Matrix Algorithm for Resonant Multiple Scattering: Applications to Localized Plasmon Excitation. *J. Opt. Soc. Am. A* **2008**, *25*, 2549–2557.

[2] Zander, C., Enderlein J. & Keller, R. A. Single-Molecule Detection in Solution - Methods and Applications, VCH-Wiley, Berlin/New York, 2002.

[3] Punj D., Optical antennas for single molecule fluorescence detection at physiological concentration, PhD thesis Aix Marseille University, 2014. https://tel.archives-ouvertes.fr/tel-01119033

[4] Ghenuche, P.; de Torres, J.; Ferrand, P.; Wenger, J. Multi-focus parallel detection of fluorescent molecules at picomolar concentration with photonic nanojets arrays. *Appl. Phys. Lett.* **2014**, *105*, 131102.

[5] Punj, D.; de Torres, J.; Rigneault, H.; Wenger, J. Gold nanoparticles for enhanced single molecule fluorescence analysis at micromolar concentration. *Opt. Express* **2013**, *21*, 27338-27343.

[6] Wenger, J.; Punj, D.; Rigneault, H. Single gold nanoparticles to enhance the detection of single fluorescent molecules at micromolar concentration using fluorescence correlation spectroscopy. *SPIE Photonics Europe* **2014**, 91261N.